Genomics 113 (2021) 3439–3448

Contents lists available at ScienceDirect

Genomics

journal homepage: www.elsevier.com/locate/ygeno

Mechanisms of responsiveness to and resistance against trabectedin in murine models of human myxoid liposarcoma

Laura Mannarino [a,b,1], Ilaria Craparotta [c,1], Sara Ballabio [c,2], Roberta Frapolli [c], Marina Meroni [c], Ezia Bello [c], Nicolò Panini [c], Maurizio Callari [d], Roberta Sanfilippo [e], Paolo G. Casali [e], Marta Barisella [f], Chiara Fabbroni [e], Sergio Marchini [b,3], Maurizio D'Incalci [a,b,3,*]

[a] Department of Biomedical Sciences, Humanitas University, via Rita Levi Montalcini 4, 20072 Pieve Emanuele - Milan, Italy.
[b] Laboratory of Cancer Pharmacology, IRCCS Humanitas Research Hospital, via Manzoni 56, 20089 Rozzano - Milan, Italy.
[c] Department of Oncology, Istituto di Ricerche Farmacologiche "Mario Negri" IRCCS, via Mario Negri 2, 20156 Milan, Italy
[d] Cancer Research UK Cambridge Institute, University of Cambridge, Li Ka Shing Centre, Cambridge, UK
[e] Adult Mesenchymal Tumour Medical Oncology Unit, Fondazione IRCCS Istituto Nazionale dei Tumori, Via Venezian 1, 20133 Milan, Italy
[f] Department of Pathology, Fondazione IRCCS Istituto Nazionale dei Tumori, Milan, Italy

ARTICLE INFO

Keywords:
Myxoid liposarcoma
Trabectedin
PDX
Data integration
RNA-Seq
DNA-Seq

ABSTRACT

Myxoid liposarcoma (MLPS) is a rare soft-tissue sarcoma characterised by the expression of FUS-DDIT3 chimera. Trabectedin has shown significant clinical anti-tumour activity against MLPS. To characterise the molecular mechanism of trabectedin sensitivity and of resistance against it, we integrated genomic and transcriptomic data from treated mice bearing ML017 or ML017/ET, two patient-derived MLPS xenograft models, sensitive to and resistant against trabectedin, respectively.

Longitudinal RNA-Seq analysis of ML017 showed that trabectedin acts mainly as a transcriptional regulator: 15 days after the third dose trabectedin modulates the transcription of 4883 genes involved in processes that sustain adipocyte differentiation. No such differences were observed in ML017/ET. Genomic analysis showed that prolonged treatment causes losses in *4p15.2, 4p16.3* and *17q21.3* cytobands leading to acquired-resistance against the drug.

The results dissect the complex mechanism of action of trabectedin and provide the basis for novel combinatorial approaches for the treatment of MLPS that could overcome drug-resistance.

1. Introduction

Myxoid liposarcoma (MLPS) is a malignant soft tissue sarcoma that origins from primitive mesenchymal cells [43]. In most cases it is characterised by the translocation t(12;16)(q13;p11) resulting in the FUS-DDIT3 oncoprotein, or rarely by the translocation t(12;22)(q13;q12) resulting in the EWS-DDIT3 chimera [56]. The FUS-DDIT3 oncoprotein has been reported to inhibit the adipocyte differentiation by the downregulation of the transcription factors C/EBPα and PPARγ [36]. Although recent research suggests that FUS-DDIT3 exerts its action mainly at the epigenetic level by interacting with several chromatin regulators[10,56], the exact mechanism of action of this oncoprotein and its role in tumour maintenance are still unclear.

Radiation in combination with surgery represents the gold-standard treatment for MLPS, which however is primarily effective against localised disease. Chemotherapy is used to treat unresectable and metastatic tumours. Anthracyclines are the standard first line treatment, and in case of poor response or severe side effects, such as cardiac dysfunction, the drug of choice is trabectedin. Trabectedin, a compound of marine origin that binds to the minor groove of the DNA, was first

Abbreviations: MLPS, myxoid liposarcoma; ET, trabectedin. DOXO, doxorubicin.

* Corresponding author at: Department of Biomedical Sciences, Humanitas University, Via Rita Levi Montalcini 4, 20072 Pieve Emanuele, Milan, Italy, Laboratory of Cancer Pharmacology, IRCCS Humanitas Research Hospital, via Manzoni 56, 20089 Rozzano, Milan, Italy
E-mail address: maurizio.dincalci@hunimed.eu (M. D'Incalci).

[1] Contribute equally to this work.
[2] Fondazione IRCCS Ca' Granda – Ospedale Maggiore Policlinico – Milan, Italy.
[3] Share co-last authorship.

https://doi.org/10.1016/j.ygeno.2021.07.028
Received 3 May 2021; Received in revised form 18 June 2021; Accepted 29 July 2021
Available online 30 July 2021

approved in Europe in 2007 for the treatment of advanced soft-tissue sarcoma after failure of anthracyclines and ifosfamide [13]. In 2015 the FDA endorsed its use for the treatment of advanced pre-treated metastatic liposarcomas and leyomiosarcomas [14] [4]. Prolonged administration of trabectedin is feasible as it does not cause cumulative toxicity. However, as for most chemotherapeutics, patients develop drug-resistance.

To date, most molecular studies on MLPS have been conducted in cell lines models with all their inherent weaknesses, such as consequences of immortalisation and absence of microenvironmental components mimicking the clinical scenario. Mindful of these issues we studied the molecular mechanisms underlying both activity of trabectedin and resistance against it choosing as experimental paradigm mice bearing patient-derived xenograft models of MLPS previously characterised in our laboratory, ML017 and ML017/ET [19] [7]. The former is responsive to trabectedin and was originated from the less common and more aggressive round cell MLPS, while the latter is resistant against trabectedin and was obtained from ML017 through repeated *in vivo* treatments [7]. Our experimental design attempted to reproduce clinical treatments details and allowed us to investigate the effects of the drug at both the genomic and transcriptional levels. We showed that trabectedin mainly acts as transcriptional regulator with major effects after prolonged treatment. Acquired-resistance against it was found to be associated with the selection of specific genomic features. The multi-level integrated analysis employed here sheds light on the molecular interaction of trabectedin with MLPS which may engender ideas for therapeutic combinatorial strategies that enhance the anti-tumour and pro-differentiation effects of trabectedin.

2. Results

2.1. Experimental design and aims

A comprehensive genomic and transcriptomic map was generated from 40 tumour biopsy samples obtained from mice bearing ML017 or ML017/ET [19] [7] (Supplementary Fig. 1). Omics data was used with the following threefold rationale: i) to characterise the genomic and the transcriptomic landscape of PDX models at basal conditions helping to adjudge the extent to which they represent clinical MLPS; ii) to determine genomic alterations responsible for acquired resistance against trabectedin; iii) to explore molecular mechanisms associated with trabectedin activity.

2.2. ML017 and ML017/ET possess genomic features of clinical MLPS

The genomic landscape of the diploid genome (Supplementary Fig. 2) of tumours was analysed using the "One-Seq" technology. This uses a single library preparation to assess simultaneously the presence of genome-wide somatic copy number alterations (SCNAs) and single nucleotide variants (SNVs) in the full length sequence of 5791 coding genes and intersperse regions on the genome. We used this database to estimate the extent to which the genome of our PDX models overlaps with that from clinical MLPS.

We identified the canonical gene translocation FUS-DDIT3 in all ML017 and ML017/ET samples together with its DDIT3-FUS counterpart (Table 1). The breakpoints on both genes were at the intron level, downstream exon 7 of *FUS* and exon 1 of *DDIT3* (Supplementary Fig. 3).

The total number of SNVs identified in ML017 and ML017/ET samples at basal conditions was compared with data for cancer types in The Cancer Genome Atlas (TCGA). Consistent with the mutational load of the sarcoma (SARC) cohort [1], *i.e.* less than 100 variants per sample, our models belong to the less mutated cancer types (Supplementary Fig. 4). As to the SCNAs dataset amplifications in cytobands *13q, 8p23.3, 8q23.1* and deletions in the chromosome arm *16q* were also identified in MLPS patients (Supplementary Table 1) [22] [24].

ML017 and ML017/ET had a median number of variants of 16 and 19 per sample, respectively, irrespective of treatment schedule (Supplementary Fig. 5). Classification of variants afforded mainly missense SNVs. Both models showed a prevalence of C > T base changes, although ML017 had more transitions than transversions (Supplementary Fig. 6). While none of the genes most frequently mutated in sarcoma, such as *TP53*, *RB1*, *ATRX* were mutated in our cohort, *PTEN* and *PIK3CA,* which are specific for MLPS, were mutated in all ML017 and ML017/ET samples (Supplementary Fig. 7, Supplementary Table 2).

These SNVs and SCNAs landscapes suggest that the genome of our ML017 and ML017/ET models genuinely reflect MLPS tumours.

Table 1
DNA structural variants identified in all samples of ML017 and ML017/ET.

Chrom	Breakend	Ref	Alt	Translocation	Variant Description
chr12	57914179	G	G] chr16:31198193]	FUS-DDIT3	gene fusion and
chr16	31198192	C	C] chr12:57914180]		frameshift variant
chr12	57914182	G	[chr16:31198193 [G	DDIT3-FUS	gene fusion and
chr16	31198192	C	[chr12:57914183 [C		frameshift variant

Chrom, chromosome; Breakend, position of the breakpoint; Ref, reference base; Alt, alternate base. First two lines report the canonical FUS-DDIT3 translocation, the last two report its counterpart DDIT3-FUS.

2.3. Effects of trabectedin on genomic architecture

We focused on the effects of trabectedin on the chromosomal architecture of ML017 and ML017/ET. Tumours were characterised by gains with a mean length of 600 kbp and losses with a mean length of 2 Mbp (Supplementary Table 1). First, we compared the total number of SCNAs across all conditions to investigate whether prolonged treatment had engendered drug-induced chromosomal instability. Boxplots show at basal level a difference between ML017 and ML017/ET in the total amount of SCNAs, with a median of 741 and 1574 ($p < 0.01$), respectively (Supplementary Fig. 8). After 24 h of treatment with trabectedin or doxorubicin the total amount of SCNAs with ML017 increased to levels seem in those with ML017/ET (Supplementary Table 2).

In order to identify recurrent SCNA regions with high confidence and to overcome technical bias, we characterised SCNAs as significant by GISTIC2 algorithm only when present in all four replicates per condition. This strategy allowed the selection of only the most reproducible and consistent genomic events.

Considering the distribution of SCNAs across the different experimental conditions, regions in gains or in loss can be grouped into three distinct groups (Fig. 1). Groups I in both panel A and B of Fig. 1 include regions that are common to both models and are stable under each condition, thus they represent specific features of these PDX models. Instead, groups II are composed of gains, *i.e. 15q14, 10q24.32, 12p13.33,* or loss, *i.e. 3q26.1*, that are irremediably lost after the first dose of drug, irrespective of trabectedin or doxorubicin treatment. They represent regions of sensitivity to pharmacological treatment. Group III in panel A harbours regions acquired after treatment with trabectedin or doxorubicin. They also characterise ML017/ET under each condition, thus they represent non-specific features associated with drug treatment but not necessarily related to drug sensitivity. Otherwise, Group III in panel B is composed of regions that are specific for ML017/ET in cytobands *4p15.2, 4p16.3* and *17q21.31*. The exclusivity of these regions to ML017/ET renders them possible specific markers of acquired resistance against trabectedin.

Together this evidence highlights three genomic features: those in Group I not affected by treatment and specific of the models, those related to sensitivity to treatment with either drug, such as those in Groups II, and those in Group III specific for ML017/ET which could be

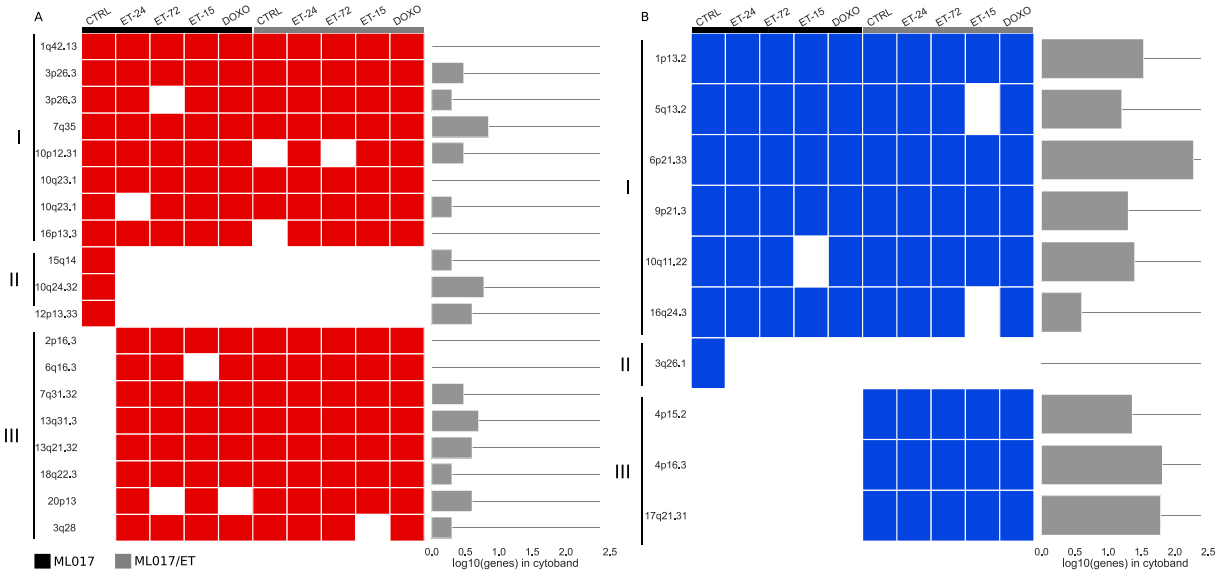

Fig. 1. SCNAs in ML017 and ML017/ET models.
Cytobands (reported on the left) interested by copy number gains (Panel A, in red) or copy number loss (Panel B, in blue) in ML017- (black) and ML017/ET- (grey) bearing mice models. Barplot on the right show the log10 number of genes in each affected region. CTRL, basal conditions; ET-24 and ET-72, 24 and 72 h after the first dose of trabectedin; ET-15, 15 days after the third dose of trabectedin; DOXO, 24 h after one dose of doxorubicin.

defined as markers of resistance.

2.4. Identification of novel variants affecting MLPS

In addition to well-known mutations in the *PTEN* and *PIK3CA* genes, we observed the genes *ANK3, CRYGB, DSC3, FAT4, IMPDH2, MUC7* and *PAK7* to harbour mutations in both models (Supplementary Fig. 9, Supplementary Table 3). All samples were characterised by the same mutated locus in each gene with comparable allelic fraction (*e.g.* the number of altered reads over the total) close to 50% (Supplementary Table 4). The high rate of shared mutations and the allelic fraction suggest the clonal nature of the tumour cells. These genes can be divided into two groups. One is composed of benign or well-tolerated variants in the *ANK3, CRYGB, FAT4* (c.9674C > A) and *MUC7* genes. The other is composed of damaging or deleterious variants in genes like *IMPDH2, DSC3, PAK7* (also known as *PAK5*) and *FAT4* (c.9678 T > A) (Supplementary Fig. 10).

A comparison of the genomes of ML017 and ML017/ET revealed differentially mutated genes specific to each model (Fig. 2): *KCNA3* was mutated in ML017 only, whilst variants of *NLGN1, UVSSA, SSTR5, SLC1A2* were exclusively seen in ML017/ET (Supplementary Table 3).

In summary, beside specific MLPS genes like *PTEN* and *PIK3CA*, we identified novel variants in the genes *IMPDH2, DSC3, PAK7* and *FAT4* (c.9678 T > A) with a possible impact on the protein structure. Comparison of the models showed that *KCNA3* is likely to be associated to trabectedin responsiveness, while variants in *NLGN1, UVSSA, SSTR5, SLC1A2* genes were selected under drug pressure in ML017/ET.

2.5. ML017 and ML017/ET present different transcriptional landscape at basal conditions

Transcriptional effects of trabectedin on the PDX models were studied using the same experimental design used for the genomic analysis. The following three approaches were taken: i. comparison of models at basal conditions to identify transcriptional markers that could explain acquired resistance; ii. study of time-dependent effects of trabectedin; iii. comparison of trabectedin with doxorubicin in terms of transcriptional effects.

In order to identify key transcriptional features that could explain drug responsiveness, we performed a differential expression analysis between ML017/ET and ML017 at basal condition. We identified 243 differentially expressed genes (DEGs) (Fig. 3 panel A, Supplementary Table 5). Of these 74 were up-regulated and 169 down-regulated and characterise the differences between the two models (Fig. 3 panel B). They were not significantly involved in any biological pathway and most belonged to the same genomic cytobands. Indeed, 63 down-regulated genes mapped on focal regions in *4p16.3*, *4p15.2* and *17q21.3*, the same cytobands of Group III in Fig. 1 panel B exclusively lost in ML017/ET model (Supplementary Table 6). Supplementary Fig. 11 shows that transcriptional down-regulation and loss of genetic material is consistent. Gene expression was not changed by drug treatment in ML017/ET suggesting they could be considered as a specific discriminant between responsiveness and resistance (Supplementary Fig. 12).

2.6. Time-dependent transcriptional effects of trabectedin

Exploration of the whole cohort of transcriptional data identified three major groups (Fig. 4). The largest group (right-bottom side) is composed of ML017 samples under CTRL, ET-24 and ET-72 conditions and of most samples from ML017/ET. Two subgroups could be distinguished, one relating to ML017 (samples indicated by triangles) and the other to ML017/ET (samples indicated by circles). The second group (depicted in orange) represents samples from animals bearing either ML017 or ML017/ET which received doxorubicin. This treatment produced similar responses in both models, in contrast to basal samples and those from mice treated with trabectedin. The third group encompasses all four replicates of ML017 obtained at 15 days after trabectedin. It suggests different transcriptional modulation at this time point exclusively in the ML017 model when compared to the other groups.

In order to identify the DEGs that characterise the groups, we studied the time-course of transcriptional modulation induced by drug treatment. We compared each time point to basal conditions per model independently. As shown in the left upper panel of Fig. 5, the strongest modulation in ML017 was elicited by trabectedin at 15 days after the third dose with 4883 DEGs. The number of DEGs at 24 and 72 h was 828 and 209, respectively (Supplementary Table 7). Genes were grouped into pathways through gene set enrichment analysis (GSEA) (Fig. 5, lower panel). Circles are coloured according to normalised enrichment

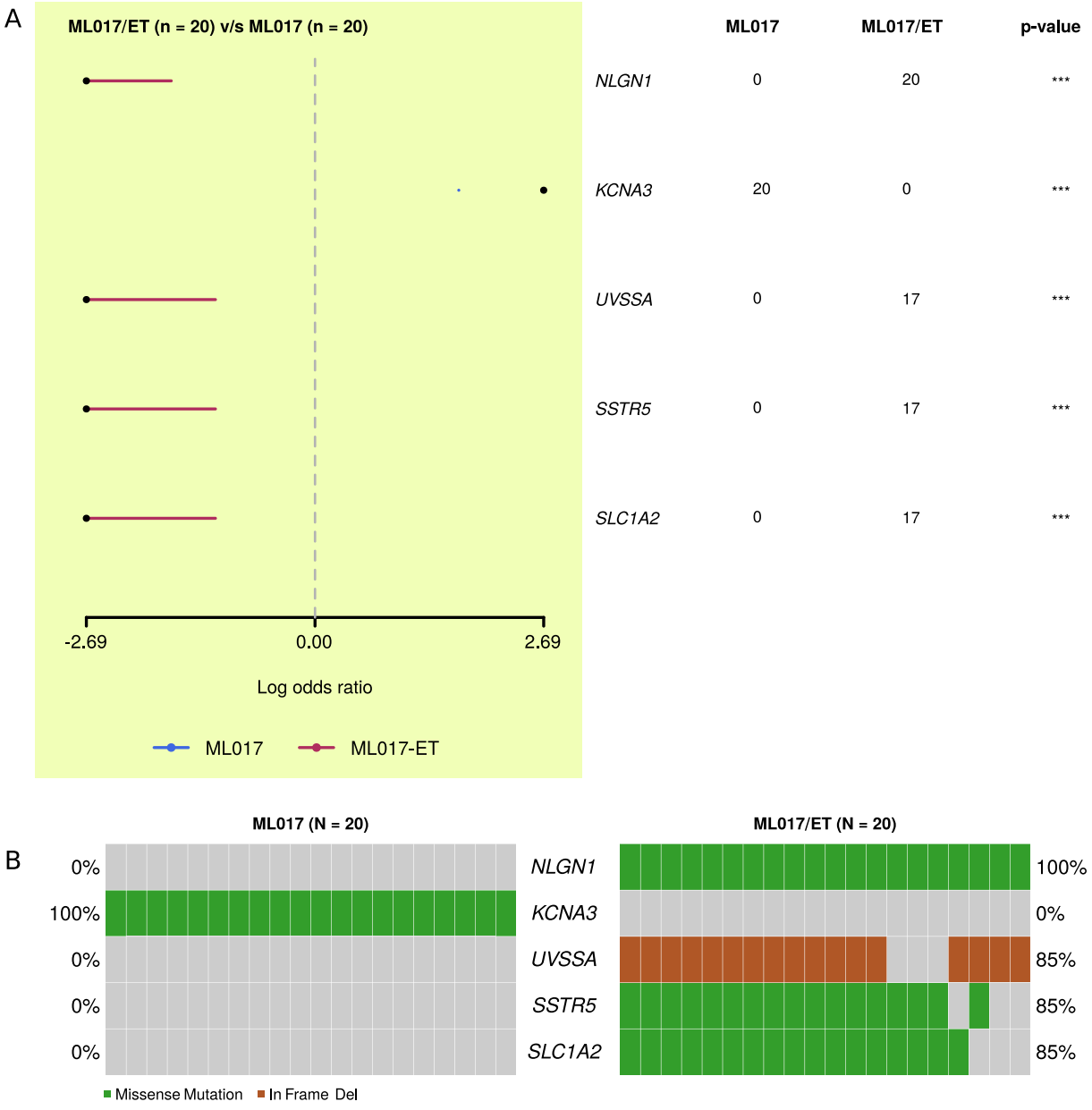

Fig. 2. Differentially mutated genes between ML017 and ML017/ET.
Panel A shows the log odds ratio of genes reported on the right. For each gene the number of samples carrying the mutation and the associated *p*-value are shown (*** less than 0.001, ** less than 0.01). Panel B shows the oncoplot of differentially mutated genes and their classification as reported in the legend.

score (NES), red in case of up-regulation and green for down-regulation. At 24 h and at 72 h, there were activated pathways related to the transcriptional regulation of TP53 and transcription. At the later time point genes were grouped into 233 pathways, of which 40 were activated and 193 inhibited, corresponding to the major transcriptional response (Supplementary Table 8). The activated pathways were mainly involved in functions that suggest structural and phenotypic changes like remodelling of extracellular matrix organisation, the production of collagen and the regulation of the insulin-like Growth Factor (IGF). Pathways germane to methylation of the DNA, the regulation of rRNAs and the pathway of the RNA polymerase I were inhibited at this time point (Supplementary Table 8). Taken together, this data is consistent with the notion that trabectedin exerts an initial cytotoxic effect whilst altering the tumour cell phenotype after prolonged treatment.

As to results for ML017/ET, the strongest response to the drug occurred at 24 h (1052 DEGs), with a weaker effect at 72 h and 15 days (219 and 3 DEGs, respectively) compared to basal conditions (right upper panel Fig. 5). At the 24 h trabectedin affected 34 pathways, with activation in 30 and inhibition in 4 cases (right bottom panel Fig. 5). Among pathways which were activated are transcriptional regulation of TP53 and RNA polymerase II, cell cycle and homology direct repair and those regulated at this time point in the ML017 tumour. At 72 h, the main effect was immune activation, while at 15 days post dosing altered pathways were not observed.

These results suggest that trabectedin induced a strong transcriptional response in ML017 mice after prolonged treatment. In contrast, in ML017/ET mice a strong response was only seen at early time points.

Doxorubicin altered transcription in both models (Supplementary Fig. 13) with a greater effect on ML017 (2420 DEGs) than ML017/ET (484 DEGs) (Supplementary Table 8). In both models, down-regulated genes were mainly associated with pathways pertinent to the cell cycle, DNA repair, Rho GTPases and regulation of cholesterol

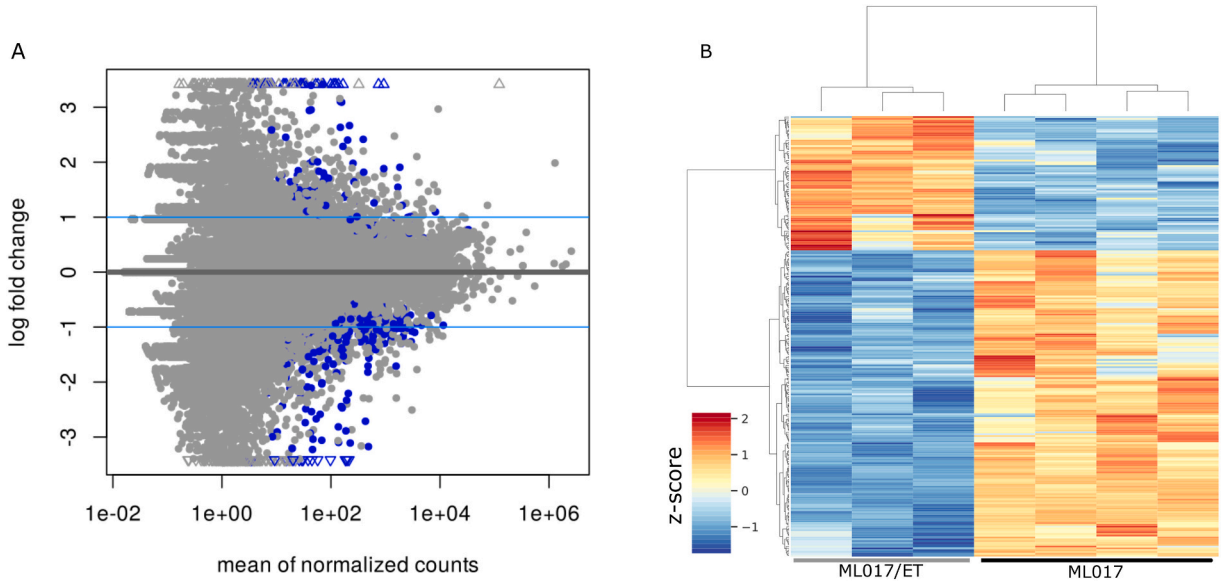

Fig. 3. Transcriptional comparison of ML017 and ML017/ET at basal condition.
Panel A shows the mean of normalised counts *versus* the log fold change associated to each gene. Points coloured in blue represent differentially expressed genes (DEGs). Panel B shows the heatmap related to the z-score of log normalised counts of the 243 DEGs (rows) in the comparison between ML017/ET and ML017 at basal conditions (columns). Colours are as reported in the legend: red for positive values, blue for negative values. Rows and columns are clustered as reported in Materials and methods.

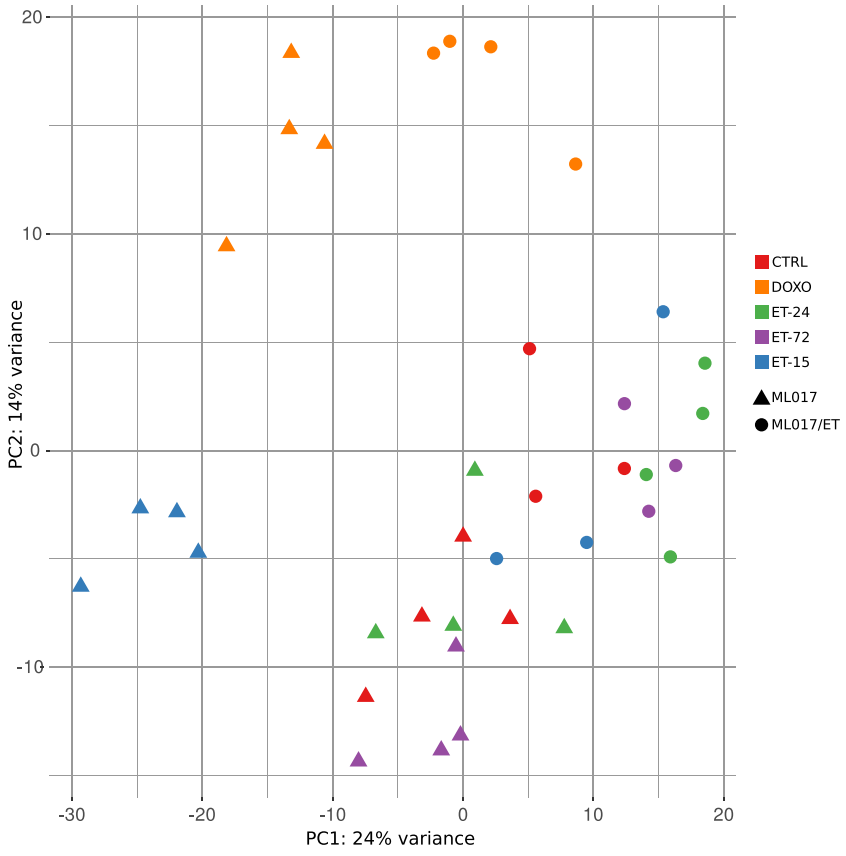

Fig. 4. Unsupervised analysis of gene counts in ML017 and ML017/ET.
Figure shows the Principal Component Analysis (PCA) of the whole cohorts ML017 and ML017/ET. Samples from ML017 are indicated with triangles, samples from ML017/ET with circles. Colours refer to conditions as reported in the legend. CTRL, basal conditions; ET-24 and ET-72, 24 and 72 h after the first dose of trabectedin; ET-15, 15 days after the third dose of trabectedin; DOXO, 24 h after one dose of doxorubicin.

biosynthesis, while the activated ones were mainly related to TP53 and extracellular matrix remodelling. Enrichment was far lower than that seen after trabectedin treatment (Supplementary Table 8).

Overall, these results suggest that the two drugs triggered different transcriptional responses. Some effects seen 24 h after administration were similar in terms of affected pathways, although involving different genes and different enrichment scores. Genes deregulated by doxorubicin in ML017/ET participated in the same biological functions as those affected in ML017, consistent with the fact that ML017/ET is sensitive to doxorubicin.

Fig. 5. Trabectedin-induced pathways over time.
Figure shows the number of differentially expressed genes (DEGs) modulated by trabectedin in ML017 model on the left or in ML017/ET on the right. Control (CTRL) is set to zero. 24 h, 72 h, 15d represent the considered time points: 24 and 72 h after the first dose and 15 days after the third dose of trabectedin. Lower panel shows most significant pathways from Gene Set Enrichment Analysis (GSEA) with Reactome database for each time point. The colour represents the normalised enrichment score (NES) as indicated in the legend: positive values for positive enrichment (up-regulation), negative values for negative enrichment (down-regulation). Radius of the circles is proportional to the number of genes in the pathways.

2.7. Discovering yet unknown transcript modulation

We wished to investigate whether trabectedin engages transcriptional mechanisms which have not yet been described. To this end, we customised the Tuxedo protocol [37] for transcript-level analysis (Supplementary Fig. 14) as explained under Materials and Methods.

The number of known transcripts were similar under each condition in ML017 (mean of 82705.3) and ML017/ET (mean of 83630.47) (Supplementary Table 9). The mean number of unknown transcripts under ET-15 conditions in ML017 was 90856.75, and under other conditions 73558.81. The equivalent number under ET-15 conditions for ML017/ET was 54337.67. Even though the amount of identified known transcripts was similar across conditions and models, major differences occurred at novel transcript level, especially in ML017 at 15 days.

In order to investigate further the effects of trabectedin treatment, we made a differential expression analysis based on transcript counts. The transcriptional differences are shown in Supplementary Fig. 15. The number of differentially expressed transcripts (DETs) followed the same trend as that seen in the gene level analysis. The major transcriptional modulation was identified at 15 days after the third dose of trabectedin in ML017 with 7602 DETs (Supplementary Table 10), thus we focused further analysis on this time point. We selected only unknown transcripts and removed those ($n = 48$) that were consistently modulated in ML017 by both trabectedin and doxorubicin at each time-point. We obtained 2719 DETs specifically related to ET-15, of which 2354 were described as possible new isoforms of already known genes most of them related to one gene (Supplementary Fig. 16). The remaining 365 were novel transcripts and because of their 200-nucleotide length they were classified as long non-coding RNAs. The 2354 specific DETs described as potentially new isoforms were analysed with CPAT (see Materials and methods) in order to assess the probability of their translation into proteins. For 990 of them this was probable (Supplementary Table 11).

In summary, we showed that trabectedin elicits a transcriptional response at later time point that involved not yet known transcripts that are worth of further investigation.

3. Discussion

In this work we integrated genomic and transcriptomic data to investigate two PDX models of MLPS in order to evaluate the molecular features responsible for sensitivity to and resistance against trabectedin. These results can be summarised as follows: i. from a molecular point of view, *in vivo* models ML017 and ML017/ET mirror the biological

features of MLPS tumour in the clinic, thus they can be considered suitable models of MLPS; ii. at the transcriptional level, the pleiotropic effects of trabectedin are time-dependent and can be divided into two phases, an early cytotoxic followed by a delayed differentiation effect; iii. the molecular mechanisms responsible for acquired resistance against trabectedin could be associated with loss of the three genomic regions *4p15.2*, *4p16.3* and *17q21.31*.

MLPS is an uncommon disease and epidemiological and clinical studies of it are rare [8]. In clinical trials MLPS is usually studied together with other sarcomas, thus the effectiveness of treatments specifically against this malignancy are masked and indeterminable [4]. In the light of the above, the use of PDX models represents a precious means in preclinical cancer research. The ML017 model was derived from a patient affected with the aggressive form of MLPS known as round cell MLPS who did not receive any previous treatment as described in Frapolli et al. [19]. ML017 proved high sensitivity to trabectedin treatment that made it suitable for the 2-years development of its resistant counterpart ML017/ET [7]. Given this premise, the models used in this work are a valuable tool to study the sensitivity to and the resistance against trabectedin and may be useful to test new treatment strategies.

Although considerable research efforts have focussed on the characterisation of MLPS, molecular details of its response to drug treatment have to our knowledge not been published. Our results suggest that in ML017-bearing mice trabectedin elicits strong transcriptional modulation 15 days after the third dose, whilst failing to induce substantial genomic alterations. At this timepoint we found remodelling of the extracellular matrix, the production of collagen, the formation of elastic fibres and the regulation of the insulin-like Growth Factor (IGF). These effects suggest that trabectedin is able to induce a phenotypic change in MLPS cells leading to the reactivation of adipocytic differentiation. This molecular evidence is consistent with morphological changes identified *in vitro* and *in vivo* previously [17]. The transformation of precursors mesenchymal cells into fully differentiated adipocytes is regulated by the interaction between the PPARγ and C/EBPα transcription factors, and in MLPS this process is blocked by FUS-DDIT3 [36]. Here, we showed that trabectedin modulates the transcriptional activity of MLPS initiating the recovery of adipocytic differentiation. Although a study has proposed a direct effect of trabectedin on the chimera [15], the role of FUS-DDIT3 in this process is unclear. Recent works have shown a strong interaction of the FUS-DDIT3 with other proteins, such as the SWI/SNF chromatin remodelling complex that is followed by altered gene expression [28,56]. The study of the modulation of the FUS-DDIT3 genome-wide binding to the DNA followed by trabectedin treatment using ChIP-Seq approach is currently in progress to define the selective mechanism of action of the drug in MLPS more precisely.

TP53 mutations in MLPS are rare and justify the sensitivity of these tumours to treatment with drugs like trabectedin or doxorubicin [39]. Indeed, the first response seen at early time points in ML017 was the cytotoxic effects elicited by the canonical activation of TP53 and MAPK pathways. In the resistant model ML017/ET trabectedin elicited a transcriptional response only at 24 h, probably due to an early cytotoxic effect. Transcriptional effects on adipocyte differentiation were observed later in ML017 and not in ML017/ET, confirming the unique mechanism of action of trabectedin. In this light, ML017/ET model might be a useful means to explore the use of drug combinations to overcome drug-resistance.

Acquired drug-resistance in cancer cells involves cellular and molecular mechanisms which ultimately lead to clinical relapse and tumour progression [53]. In MLPS these mechanisms are still unknown [18] [3,29]. ML017 and ML017/ET had differentially mutated genes, *KCNA3* in ML017 and variants in *NLGN1*, *UVSSA*, *SSTR5*, *SLC1A2* in ML017/ET. Cytobands *4p15.2*, *4p16.3* and *17q21.31* were specifically lost in ML017/ET. Since ML017/ET was established through continuous passages in mice following a strict schedule of trabectedin treatment [7], these three regions might have been lost upon drug pressure. The specificity of their loss for ML017/ET identifies them as features of sensitivity to trabectedin the loss of which engendering resistance against the drug. Among the genes mapped on the lost band *4p16.3* there was *UVSSA* that carries an in-frame deletion. *UVSSA* (UV-stimulated scaffold protein A) is involved in the Transcription-Coupled Nucleotide Excision Repair (TC-NER), a mechanism that removes helix-distorting lesions from the genome [51]. Loss of *UVSSA*, even if compatible with cell growth [45], leads to deficient TC-NER [20]. Cells with defective TC-NER are resistant to trabectedin treatment[4,26]. The absence of *UVSSA* in ML017/ET, that has been observed before [7], might well be implicated in trabectedin-induced acquired resistance. The knowledge of the molecular mechanism associated with drug resistance can support future development of combinatorial therapeutic strategies that can reactivate the differentiation program *via* different pathways as in the case of pioglitazone [18].

Differences between ML017 and ML017/ET at the genomic level were accompanied by differential transcriptional regulation. We identified 243 DEGs. Although none of them could be linked to specific biological functions, most mapped onto chromosomal regions *4p16.3*, *4p15.2* and *17q21.3* which were lost in ML017/ET. This result suggests that the loss of this genetic material corresponds to a coherent change of transcriptional activity and commends *4p16.3, 4p15.2* and *17q21.3* as specific markers of sensitivity to trabectedin.

In conclusion, our comprehensive study of two MLPS models characterises the pharmacogenomics of trabectedin in relation to the sensitivity to and resistance against this drug in MLPS. The genomic losses in *4p16.3*, *4p15.2* and *17q21.3* represent a novel insight into the mechanism of resistance that warrant further investigation. Moreover, late transcriptional responses to trabectedin leading to differentiation provide new knowledge of potential clinical relevance, thus being of help to design novel therapeutic strategies to enhance tumour response.

4. Materials and methods

4.1. Animals

Six- to eight-week-old female CD1 nude mice were obtained from Charles River Laboratories (Calco, Italy) and housed in individually ventilated cages with sterilized food and water *ad libitum* and handled under specific pathogen-free conditions in the Animal Care Facility of the Mario Negri Institute which meets international standards. Mice were regularly checked by a certified veterinarian who is responsible for health monitoring, animal welfare supervision, experimental protocols and review of procedures. Procedures involving animals and their care were conducted in conformity with the following laws, regulations, and policies governing the care and use of laboratory animals: Italian Governing Law (D.lgs 26/2014; Authorization n.19/2008-A issued March 6, 2008, by the Ministry of Health); Mario Negri Institutional Regulations and Policies providing internal authorisation for persons conducting animal experiments (Quality Management System Certificate—UNI EN ISO 9001:2008—Reg. No. 6121); the NIH Guide for the Care and Use of Laboratory Animals (2011 edition) and EU directives and guidelines (EEC Council Directive 2010/63/UE), and in line with guidelines for the welfare and use of animals in cancer research [54].

4.2. Drugs

Trabectedin (Yondelis®, ET743) was kindly supplied by PharmaMar, S.A. (Colmenar Viejo, Spain). They were dissolved in water and further diluted in saline immediately before use. Doxorubicin (SANDOZ clinical formulation) was diluted with water immediately before use.

4.3. Tumour models

The ML017 patient-derived round-cell myxoid liposarcoma xenograft was maintained through serial transplantation in mice, as

previously described [19]. Briefly, tumours from donor mice were cut into small fragments of about 3 × 3 mm that were engrafted subcutaneously in female athymic nude mice under isoflurane anaesthesia. The maintenance of the original histological features of the tumours grown was verified to maintain the clinical relevance of the model. ML017/ET was obtained from ML017 through repeated *in vivo* treatment with trabectedin until acquiring a resistant phenotype as described in Bello et al. [7]. When tumour burden reached about 300 to 400 mg, mice bearing ML017 or ML017/ET xenografts were randomised to receive trabectedin 0.15 mg/kg intra-venously, every 7 days for three times (q7dX3) or doxorubicin 8 mg/kg i.v. every 7 days for two times (q7dx2). Tumour growth was measured using Vernier caliper, and tumour weights were calculated by the formula: length x (width)2/2.

4.4. FACS analysis

DNA analysis content was performed in tumour cells derived from *in vivo* models. The two tumour tissues ML017 and ML017/ET were mechanically disaggregated by MediMachine (BD Biosciences, Franklin Lakes, New Jersey, USA). After disaggregation of the tissue, the cell suspension was filtered using a 100 μm CellTrics disposable filter (Sysmex Europe, GmbH, Bornbarch, Norderstedt, Germania) and then fixed with 70% Ethanol.

After at least 4 h in ethanol, 2×10^6 cells were incubated over night at 4 °C with 1 ml of Propidium Iodide 25 μg/ml (Calbiochem, Merck Burlington, Massachusetts, USA) and 12.5 μl of RNAse 1 mg/ml (Calbiochem, Merck Burlington, Massachusetts, USA) in PBS. DNA analysis was performed with a Beckton Dikinson FACSCalibur flow cytometer (BD Biosciences, Franklin Lakes, New Jersey, USA) equipped with blue (488 nm) and red (630 nm) lasers. To construct each histogram 10.000–20.000 cells were analysed for ploidy evaluation. Instrument was calibrated with an aliquot of peripheral blood mononuclear cell (PBMNC) that was also used as an internal diploid standard. Aneuploidy was estimated by the DNA index value, calculated as the ratio between the modal channel of the G0/G1 peak of the sample under study and the modal channel of the G0/G1 peak of the reference standard. For a diploid cell population the DNA index is 1.00.

4.5. DNA and RNA extraction

gDNA and total RNA were extracted from tumour specimens with the QIAamp DNA Mini kit and (QIAGEN, Hilden, Germany) and the miRNeasy Mini kit (QIAGEN, Hilden, Germany) respectively, following protocols' instructions and using an automatic nucleic acid purification system (Qiacube, QIAGEN, Hilden, Germany).

Before library preparation, gDNA and RNA concentration were evaluated using Qubit® dsDNA High Sensitivity Assay Kit and Qubit™ RNA High Sensitivity Assay Kit (Invitrogen, Carlsbad, California, USA) respectively, while the quality was established using 4200 Tapestation (Agilent Technologies, Santa Clara, California, USA).

4.6. DNA and RNA sequencing

200 ng of DNA were sheared on Bioruptor (Diagenode, Seraing (Ougrée), Belgium) then purified with AMPure XP beads (Beckman Coulter, Brea, California, USA). Following the Sure Select XT protocol (Agilent Technologies, Santa Clara, California, USA), libraries were generated using the Bravo automatic liquid handling station (Agilent Technologies, Santa Clara, California, USA). OneSeq Constitutional Research Panel (Agilent Technologies) was used as capture probes to determine structural variants and mutations of 5791 disease-related genes. After the last AMPure XP beads purification, samples were examined for quality and quantity and the sequencing run was done on a NextSeq 500 sequencer (Illumina San Diego, California, USA) using a 2 × 150 high-output flow cell with 15 samples/run.

Following the TruSeq Stranded Total RNA protocol, 500 ng of RNA with RIN value between 6 and 9 was sequenced. Libraries with optimal quality and quantity were run on NextSeq 500 sequencer (Illumina San Diego, California, USA) using a 2 × 150 high-output flow cell with 6 samples/run.

4.7. High throughput sequencing data analysis

4.7.1. Data pre-processing

Raw sequences were demultiplexed with bcl2fastq Conversion Software (Illumina [6]) using *–no-lane-splitting* parameter, obtaining two reads per sample. FastQC [5]) was used for quality control of *fastq* files that were simultaneously visualised through MultiQC [16].

4.7.2. DNA-Sequencing

For DNA-Sequencing analysis we used a public available pipeline named bcbio-nextgen [12] that was configured and run on an in-house high-performance computing platform. Raw reads were aligned on *hg19* human genome with BWA-MEM aligner [27] version 0.7.17. Sequencing generated a mean of 55.48 M reads per sample with a mean coverage of 91.82×. In order to avoid mouse genome contamination we filtered out mouse sequencing reads (*mm10* genome version) with disambiguate software [2]. Somatic variants were called matching each tumour to the healthy sample and retained when called by both MuTect2 [11] version 1.1.5 and VarDict [25] variant callers. For variant impact prediction we used: PolyPhen [41], SIFT [33], CADD [42]. *vcf* (Variant Call Format) files were stored in a GEMINI database [34] that was converted into a MAF (Mutation Annotation Format). Maftools [31] was used for data visualisation and identification of differentially mutated genes. Lolliplots were done with trackViewer [50]. Somatic Copy Number Alterations calling was done through CNVkit [49] version 0.9.4. GISTIC2.0 [32] was used to define frequent altered regions in the whole cohort of ML017 and ML017/ET samples. GISTIC2.0 was run under both broad and focal configurations with default settings. In order to define altered regions specific of each condition, regions were retained when called as significant in all four replicates for each condition. Genomic data visualisation was done with the Integrative Genome Viewer (IGV) [44].

4.7.3. RNA-Sequencing

4.7.3.1. Gene-level analysis. In order to remove RNA reads from the mouse genome, we used the *In silico Combined human-mouse Reference Genome* (ICGR [9]) approach combining *hg19* human genome and *mm10* mouse genome with hisat2 aligner [23]. Then, we selected human aligned reads only and used bcbio-nextgen pipeline [12]. Post-alignment quality control was performed with bcbioRNASeq [47] and based on quality parameters we removed from further analysis a total of three samples from ML017/ET, one from CTRL, ET-72 and ET-15 conditions each. Gene counts were computed with the wicked-fast inference algorithm of Salmon [35]. Then, salmon quantification was read with tximport [46]. Differential expression analysis was done with DESeq2 package [30] contrasting each treatment condition with controls in each model, independently, or contrasting the basal conditions of ML017/ET *versus* ML017. Differentially expressed genes (DEGs) were filtered with a p-adjust less than 0.05. Pathway analysis was done using clusterProfiler package [55] performing the Gene Set Enrichment Analysis (GSEA [48]) sorting genes according to their log2 Fold Change, from the most up-regulated to the most down-regulated, with the Reactome database [21]. Clustering of the z-score normalised log values of gene counts was done with Ward variance minimisation algorithm.

4.7.3.2. Transcript-level analysis. For transcript-level analysis and identification of novel isoforms, we adapted the Tuxedo protocol presented in Pertea et al. [37]. Specifically, we aligned raw sequencing reads with hisat2 aligner [23], then we used StringTie [38] for

transcripts assembly and quantification with *hg19* annotation file. Then, we used gffcompare [37] to determine the number of transcripts matching the annotation. Next, we used the *merge* function of StringTie that merges transcripts from all samples in a consistent set. Finally, using aligned files and merged transcripts previously identified, we quantified transcripts through the *-e—B* mode of StringTie. The table of transcripts counts was created with prepDE.py [40] a Python script provided by the StringTie documentation. The transcripts count matrix was loaded and analysed with DESeq2 package ([30], p. 2). Differential expression analysis was done contrasting each treatment condition with controls in each model, independently. Differentially expressed transcripts (DETs) were filtered with a p-adjust less than 0.05. Transcripts were annotated accordingly to StringTie annotation file. Coding potential of novel identified isoforms was predicted with the Coding-Potential Assessment Tool (CPAT [52]).

Supplementary data to this article can be found online at https://doi.org/10.1016/j.ygeno.2021.07.028.

Ethics approval and consent to participate

Experimental protocols have been reviewed and approved by the IRFMN Animal Care and Use Committee (IACUC), that includes members *ad hoc* for ethical issues, and by the Italian Ministry of Health.

Competing interests

The authors declare that they have no competing interests.

Funding information

This work was supported by the Italian Association for Cancer Research grant to M. D'Incalci (Project Number 19189). This research was partially supported by the Guido Berlucchi Foundation.

Credit author statement

Laura Mannarino, Ilaria Craparotta: Data Curation, Writing - Original Draft - Review & Editing. Laura Mannarino: Software, Formal analysis, Visualization. Ilaria Craparotta, Sara Ballabio: Sequencing experiments. Roberta Frapolli, Marina Meroni, Ezia Bello: Experimental design, Patient-derived xenograft management. Nicolò Panini: FACS facility. Maurizio Callari: Bioinformatics Supervision. Roberta Sanfilippo, Paolo G. Casali, Marta Barisella, Chiara Fabbroni: Sample collection, Clinical and Pathological Supervision. Sergio Marchini, Maurizio D'Incalci: Conceptualization, Data Curation, Writing - Original Draft - Review & Editing, Supervision. Maurizio D'Incalci: Funding acquisition. Multiple authors contributed in Materials and methods section. All the authors: Review & Editing, Approval of the final manuscript.

Acknowledgements

We would like to thank Andreas Gescher and Ilaria Fuso Nerini for critical revision and editing of the article, Florian Markowetz for advice on data analysis. We are grateful to "Cloud4CARE" project for providing computational resources.

References

[1] A. Abeshouse, C. Adebamowo, S.N. Adebamowo, R. Akbani, T. Akeredolu, A. Ally, M.L. Anderson, P. Anur, E.L. Appelbaum, J. Armenia, J.T. Auman, M.H. Bailey, L. Baker, M. Balasundaram, S. Balu, F.P. Barthel, J. Bartlett, S.B. Baylin, M. Behera, D. Belyaev, J. Bennett, C. Benz, R. Beroukhim, M. Birrer, T. Bocklage, T. Bodenheimer, L. Boice, M.S. Bootwalla, J. Bowen, R. Bowlby, J. Boyd, A. S. Brohl, D. Brooks, L. Byers, R. Carlsen, P. Castro, H.-W. Chen, A.D. Cherniack, F. Chibon, L. Chin, J. Cho, E. Chuah, S. Chudamani, C. Cibulskis, L.A. Cooper, L. Cope, M.G. Cordes, D. Crain, E. Curley, L. Danilova, F. Dao, I.J. Davis, L.E. Davis, T. Defreitas, K. Delman, J.A. Demchok, G.D. Demetri, E.G. Demicco, N. Dhalla, L. Diao, L. Ding, P. DiSaia, P. Dottino, L.A. Doyle, E. Drill, M. Dubina, J. Eschbacher, K. Fedosenko, I. Felau, M.L. Ferguson, S. Frazer, C.C. Fronick, V. Fulidou, L.A. Fulton, R.S. Fulton, S.B. Gabriel, J. Gao, Q. Gao, J. Gardner, J. M. Gastier-Foster, C.M. Gay, N. Gehlenborg, M. Gerken, G. Getz, A.K. Godwin, E. M. Godwin, E. Gordienko, J.E. Grilley-Olson, D.A. Gutman, D.H. Gutmann, D. N. Hayes, A.M. Hegde, D.I. Heiman, Z. Heins, C. Helsel, A.J. Hepperla, K. Higgins, K.A. Hoadley, S. Hobensack, R.A. Holt, D.B. Hoon, J.L. Hornick, A.P. Hoyle, X. Hu, M. Huang, C.M. Hutter, M. Iacocca, D.R. Ingram, M. Ittmann, L. Iype, S.R. Jefferys, K.B. Jones, C.D. Jones, S.J. Jones, T. Kalir, B.Y. Karlan, A. Karseladze, K. Kasaian, J. Kim, R. Kundra, H. Kuo, M. Ladanyi, P.H. Lai, P.W. Laird, E. Larsson, M. S. Lawrence, A.J. Lazar, S. Lee, D. Lee, K.-V. Lehmann, K.M. Leraas, J. Lester, D. A. Levine, I. Li, T.M. Lichtenberg, P. Lin, J. Liu, W. Liu, E.M. Liu, L. Lolla, Y. Lu, Y. Ma, R. Madan, D.T. Maglinte, A. Magliocco, R.G. Maki, D. Mallery, G. Manikhas, E.R. Mardis, A. Mariamidze, M.A. Marra, J.A. Martignetti, C. Martinez, M. Mayo, M.D. McLellan, S. Meier, S. Meng, M. Meyerson, P.A. Mieczkowski, C.A. Miller, G. B. Mills, R.A. Moore, S. Morris, L.E. Mose, E. Mozgovoy, A.J. Mungall, K. Mungall, M. Nalisnik, R. Naresh, Y. Newton, M.S. Noble, J.E. Novak, A. Ochoa, N. Olvera, T. K. Owonikoko, O. Paklina, J. Parfitt, J.S. Parker, A. Pastore, J. Paulauskis, R. Penny, E. Pereira, C.M. Perou, A.H. Perou, T. Pihl, R.E. Pollock, O. Potapova, A. J. Radenbaugh, S.S. Ramalingam, N.C. Ramirez, W.K. Rathmell, C.P. Raut, R. F. Riedel, C. Reilly, S.M. Reynolds, J. Roach, A.G. Robertson, J. Roszik, B.P. Rubin, S. Sadeghi, G. Saksena, A. Salner, F. Sanchez-Vega, C. Sander, J.E. Schein, H. K. Schmidt, N. Schultz, S.E. Schumacher, H. Sekhon, Y. Senbabaoglu, G. Setdikova, C. Shelton, T. Shelton, R. Shen, Y. Shi, J. Shih, I. Shmulevich, G.L. Sica, J. V. Simons, S. Singer, P. Sipahimalani, T. Skelly, N. Socci, H.J. Sofia, M.G. Soloway, P. Spellman, Q. Sun, P. Swanson, A. Tam, D. Tan, R. Tarnuzzer, N. Thiessen, E. Thompson, L.B. Thorne, P. Tong, K.E. Torres, M. van de Rijn, D.J. Van Den Berg, B.A. Van Tine, U. Veluvolu, R. Verhaak, D. Voet, O. Voronina, Y. Wan, Z. Wang, J. Wang, J.N. Weinstein, D.J. Weisenberger, M.D. Wilkerson, R.K. Wilson, L. Wise, T. Wong, W. Wong, J. Wrangle, Y. Wu, M. Wyczalkowski, L. Yang, C. Yau, V. Yellapantula, J.C. Zenklusen, Zhang, J. (Julia), Hailei Zhang, Hongxin Zhang, E. Zmuda, Comprehensive and integrated genomic characterization of adult soft tissue sarcomas, Cell 171 (2017) 950–965, e28, https://doi.org/10.1016/j.cell.2017.10.014.

[2] M.J. Ahdesmäki, S.R. Gray, J.H. Johnson, Z. Lai, Disambiguate: an open-source application for disambiguating two species in next generation sequencing data from grafted samples, F1000Res 5 (2016) 2741, https://doi.org/10.12688/f1000research.10082.2.

[3] P. Allavena, G. Germano, C. Belgiovine, M. D'Incalci, A. Mantovani, Trabectedin, OncoImmunology 2 (2013), e24614, https://doi.org/10.4161/onci.24614.

[4] T. Assi, J. Kattan, E. El Rassy, C. Honore, S. Dumont, O. Mir, A. Le Cesne, A comprehensive review of the current evidence for trabectedin in advanced myxoid liposarcoma, Cancer Treat. Rev. 72 (2019) 37–44, https://doi.org/10.1016/j.ctrv.2018.11.003.

[5] Babraham Bioinformatics, FastQC A Quality Control tool for High Throughput Sequence Data [WWW Document], n.d. URL, https://www.bioinformatics.babraham.ac.uk/projects/fastqc/, 2021 (accessed 10.20.20).

[6] bcl2fastq Conversion Software, WWW Document, n.d. URL, https://emea.support.illumina.com/sequencing/sequencing_software/bcl2fastq-conversion-software.html, 2021 (accessed 10.20.20).

[7] E. Bello, S. Brich, I. Craparotta, L. Mannarino, S. Ballabio, R. Gatta, S. Marchini, L. Carrassa, C. Matteo, R. Sanfilippo, A. Gronchi, P.G. Casali, S. Pilotti, M. D'Incalci, R. Frapolli, Establishment and characterisation of a new patient-derived model of myxoid liposarcoma with acquired resistance to trabectedin, Br. J. Cancer 121 (2019) 464–473, https://doi.org/10.1038/s41416-019-0550-2.

[8] S. Bock, D.G. Hoffmann, Y. Jiang, H. Chen, D. Il'yasova, Increasing incidence of liposarcoma: a population-based study of national surveillance databases, 2001–2016, Int. J. Environ. Res. Public Health (2020) 17, https://doi.org/10.3390/ijerph17082710.

[9] M. Callari, A.S. Batra, R.N. Batra, S.-J. Sammut, W. Greenwood, H. Clifford, C. Hercus, S.-F. Chin, A. Bruna, O.M. Rueda, C. Caldas, Computational approach to discriminate human and mouse sequences in patient-derived tumour xenografts, BMC Genomics 19 (2018) 19, https://doi.org/10.1186/s12864-017-4414-y.

[10] Y. Chen, L. Xu, A. Mayakonda, M.-L. Huang, D. Kanojia, T.Z. Tan, P. Dakle, R.Y.-T. Lin, X.-Y. Ke, J.W. Said, J. Chen, S. Gery, L.-W. Ding, Y.-Y. Jiang, A. Pang, M. E. Puhaindran, B.C. Goh, H.P. Koeffler, Bromodomain and extraterminal proteins foster the core transcriptional regulatory programs and confer vulnerability in liposarcoma, Nat. Commun. 10 (2019) 1353, https://doi.org/10.1038/s41467-019-09257-z.

[11] K. Cibulskis, M.S. Lawrence, S.L. Carter, A. Sivachenko, D. Jaffe, C. Sougnez, S. Gabriel, M. Meyerson, E.S. Lander, G. Getz, Sensitive detection of somatic point mutations in impure and heterogeneous cancer samples, Nat. Biotechnol. 31 (2013) 213–219, https://doi.org/10.1038/nbt.2514.

[12] Contents — bcbio-nextgen 1.2.4 Documentation, WWW Document, n.d. URL, https://bcbio-nextgen.readthedocs.io/en/latest/, 2021 (accessed 10.21.20).

[13] G.D. Demetri, S.P. Chawla, M. von Mehren, P. Ritch, L.H. Baker, J.Y. Blay, K. R. Hande, M.L. Keohan, B.L. Samuels, S. Schuetze, C. Lebedinsky, Y.A. Elsayed, M. A. Izquierdo, J. Gómez, Y.C. Park, A. Le Cesne, Efficacy and safety of trabectedin in patients with advanced or metastatic liposarcoma or leiomyosarcoma after failure of prior anthracyclines and ifosfamide: results of a randomized phase II study of two different schedules, J. Clin. Oncol. 27 (2009) 4188–4196, https://doi.org/10.1200/JCO.2008.21.0088.

[14] G.D. Demetri, M. von Mehren, R.L. Jones, M.L. Hensley, S.M. Schuetze, A. Staddon, M. Milhem, A. Elias, K. Ganjoo, H. Tawbi, B.A. Van Tine, A. Spira, A. Dean, N. Z. Khokhar, Y.C. Park, R.E. Knoblauch, T.V. Parekh, R.G. Maki, S.R. Patel, Efficacy and safety of trabectedin or dacarbazine for metastatic liposarcoma or

leiomyosarcoma after failure of conventional chemotherapy: results of a phase III randomized multicenter clinical trial, J. Clin. Oncol. 34 (2016) 786–793, https://doi.org/10.1200/JCO.2015.62.4734.
[15] S. Di Giandomenico, R. Frapolli, E. Bello, S. Uboldi, S.A. Licandro, S. Marchini, L. Beltrame, S. Brich, V. Mauro, E. Tamborini, S. Pilotti, P.G. Casali, F. Grosso, R. Sanfilippo, A. Gronchi, R. Mantovani, R. Gatta, C.M. Galmarini, J.M.F. Sousa-Faro, M. D'Incalci, Mode of action of trabectedin in myxoid liposarcomas, Oncogene 33 (2014) 5201–5210, https://doi.org/10.1038/onc.2013.462.
[16] P. Ewels, M. Magnusson, S. Lundin, M. Käller, MultiQC: summarize analysis results for multiple tools and samples in a single report, Bioinformatics 32 (2016) 3047–3048, https://doi.org/10.1093/bioinformatics/btw354.
[17] C. Forni, M. Minuzzo, E. Virdis, E. Tamborini, M. Simone, M. Tavecchio, E. Erba, F. Grosso, A. Gronchi, P. Aman, P. Casali, M. D'Incalci, S. Pilotti, R. Mantovani, Trabectedin (ET-743) promotes differentiation in myxoid liposarcoma tumors, Mol. Cancer Ther. 8 (2009) 449–457, https://doi.org/10.1158/1535-7163.MCT-08-0848.
[18] R. Frapolli, E. Bello, M. Ponzo, I. Craparotta, L. Mannarino, S. Ballabio, S. Marchini, L. Carrassa, P. Ubezio, L. Porcu, S. Brich, R. Sanfilippo, P.G. Casali, A. Gronchi, S. Pilotti, M. D'Incalci, Combination of PPARγ agonist pioglitazone and trabectedin induce adipocyte differentiation to overcome trabectedin resistance in myxoid liposarcomas, Clin. Cancer Res. 25 (2019) 7565–7575, https://doi.org/10.1158/1078-0432.CCR-19-0976.
[19] R. Frapolli, E. Tamborini, E. Virdis, E. Bello, E. Tarantino, S. Marchini, F. Grosso, R. Sanfilippo, A. Gronchi, J.C. Tercero, G. Peloso, P. Casali, S. Pilotti, M. D'Incalci, Novel models of myxoid liposarcoma xenografts mimicking the biological and pharmacologic features of human tumors, Clin. Cancer Res. 16 (2010) 4958–4967, https://doi.org/10.1158/1078-0432.CCR-10-0317.
[20] M. Higa, K. Tanaka, M. Saijo, Inhibition of UVSSA ubiquitination suppresses transcription-coupled nucleotide excision repair deficiency caused by dissociation from USP7, FEBS J. 285 (2018) 965–976, https://doi.org/10.1111/febs.14382.
[21] B. Jassal, L. Matthews, G. Viteri, C. Gong, P. Lorente, A. Fabregat, K. Sidiropoulos, J. Cook, M. Gillespie, R. Haw, F. Loney, B. May, M. Milacic, K. Rothfels, C. Sevilla, V. Shamovsky, S. Shorser, T. Varusai, J. Weiser, G. Wu, L. Stein, H. Hermjakob, P. D'Eustachio, The reactome pathway knowledgebase, Nucleic Acids Res. 48 (2020) D498–D503, https://doi.org/10.1093/nar/gkz1031.
[22] D. Kanojia, Y. Nagata, M. Garg, D.H. Lee, A. Sato, K. Yoshida, Y. Sato, M. Sanada, A. Mayakonda, C. Bartenhagen, H.-U. Klein, N.B. Doan, J.W. Said, S. Mohith, S. Gunasekar, Y. Shiraishi, K. Chiba, H. Tanaka, S. Miyano, O. Myklebost, H. Yang, M. Dugas, L.A. Meza-Zepeda, A.W. Silberman, C. Forscher, J.W. Tyner, S. Ogawa, H.P. Koeffler, Genomic landscape of liposarcoma, Oncotarget 6 (2015) 42429–42444, https://doi.org/10.18632/oncotarget.6464.
[23] D. Kim, J.M. Paggi, C. Park, C. Bennett, S.L. Salzberg, Graph-based genome alignment and genotyping with HISAT2 and HISAT-genotype, Nat. Biotechnol. 37 (2019) 907–915, https://doi.org/10.1038/s41587-019-0201-4.
[24] M. Koczkowska, B.S. Lipska-Ziętkiewicz, M. Iliszko, J. Ryś, M. Miettinen, J. Lasota, W. Biernat, A. Harazin-Lechowska, A. Kruczak, J. Limon, Application of high-resolution genomic profiling in the differential diagnosis of liposarcoma, Mol. Cytogenet. 10 (2017) 7, https://doi.org/10.1186/s13039-017-0309-5.
[25] Z. Lai, A. Markovets, M. Ahdesmaki, B. Chapman, O. Hofmann, R. McEwen, J. Johnson, B. Dougherty, J.C. Barrett, J.R. Dry, VarDict: a novel and versatile variant caller for next-generation sequencing in cancer research, Nucleic Acids Res. 44 (2016), e108, https://doi.org/10.1093/nar/gkw227.
[26] A.K. Larsen, C.M. Galmarini, M. D'Incalci, Unique features of trabectedin mechanism of action, Cancer Chemother. Pharmacol. 77 (2016) 663–671, https://doi.org/10.1007/s00280-015-2918-1.
[27] H. Li, R. Durbin, Fast and accurate short read alignment with burrows-wheeler transform, Bioinformatics 25 (2009) 1754–1760, https://doi.org/10.1093/bioinformatics/btp324.
[28] M. Lindén, C. Thomsen, P. Grundevik, E. Jonasson, D. Andersson, R. Runnberg, S. Dolatabadi, C. Vannas, M. Luna Santamaría, H. Fagman, A. Ståhlberg, P. Åman, FET family fusion oncoproteins target the SWI/SNF chromatin remodeling complex, EMBO Rep. 20 (2019), https://doi.org/10.15252/embr.201845766.
[29] R. Loria, V. Laquintana, G. Bon, D. Trisciuoglio, R. Frapolli, R. Covello, C. A. Amoreo, V. Ferraresi, C. Zoccali, M. Novello, D. Del Bufalo, M. Milella, R. Biagini, M. D'Incalci, R. Falcioni, HMGA1/E2F1 axis and NFkB pathways regulate LPS progression and trabectedin resistance, Oncogene 37 (2018) 5926–5938, https://doi.org/10.1038/s41388-018-0394-x.
[30] M.I. Love, W. Huber, S. Anders, Moderated estimation of fold change and dispersion for RNA-seq data with DESeq2, Genome Biol. 15 (2014) 550, https://doi.org/10.1186/s13059-014-0550-8.
[31] A. Mayakonda, D.-C. Lin, Y. Assenov, C. Plass, H.P. Koeffler, Maftools: efficient and comprehensive analysis of somatic variants in cancer, Genome Res. 28 (2018) 1747–1756, https://doi.org/10.1101/gr.239244.118.
[32] C.H. Mermel, S.E. Schumacher, B. Hill, M.L. Meyerson, R. Beroukhim, G. Getz, GISTIC2.0 facilitates sensitive and confident localization of the targets of focal somatic copy-number alteration in human cancers, Genome Biol. 12 (2011) R41, https://doi.org/10.1186/gb-2011-12-4-r41.
[33] P.C. Ng, S. Henikoff, SIFT: predicting amino acid changes that affect protein function, Nucleic Acids Res. 31 (2003) 3812–3814.
[34] U. Paila, B.A. Chapman, R. Kirchner, A.R. Quinlan, GEMINI: integrative exploration of genetic variation and genome annotations, PLoS Comput. Biol. 9 (2013), e1003153, https://doi.org/10.1371/journal.pcbi.1003153.
[35] R. Patro, G. Duggal, M.I. Love, R.A. Irizarry, C. Kingsford, Salmon provides fast and bias-aware quantification of transcript expression, Nat. Methods 14 (2017) 417–419, https://doi.org/10.1038/nmeth.4197.
[36] P.A. Pérez-Mancera, C. Bermejo-Rodríguez, M. Sánchez-Martín, F. Abollo-Jiménez, B. Pintado, I. Sánchez-García, FUS-DDIT3 prevents the development of adipocytic precursors in liposarcoma by repressing PPARgamma and C/EBPalpha and activating eIF4E, PLoS One 3 (2008), e2569, https://doi.org/10.1371/journal.pone.0002569.
[37] M. Pertea, D. Kim, G.M. Pertea, J.T. Leek, S.L. Salzberg, Transcript-level expression analysis of RNA-seq experiments with HISAT, StringTie and Ballgown, Nat. Protoc. 11 (2016) 1650–1667, https://doi.org/10.1038/nprot.2016.095.
[38] M. Pertea, G.M. Pertea, C.M. Antonescu, T.-C. Chang, J.T. Mendell, S.L. Salzberg, StringTie enables improved reconstruction of a transcriptome from RNA-seq reads, Nat. Biotechnol. 33 (2015) 290–295, https://doi.org/10.1038/nbt.3122.
[39] S. Pilotti, C. Lavarino, A. Mezzelani, C. Della Torre, F. Minoletti, G. Sozzi, A. Azzarelli, F. Rilke, M.A. Pierotti, Limited role of TP53 and TP53-related genes in myxoid liposarcoma, Tumori 84 (1998) 571–577.
[40] prepDE, WWW Document, n.d. URL, http://ccb.jhu.edu/software/stringtie/dl/prepDE.py, 2021 (accessed 10.21.20).
[41] V. Ramensky, P. Bork, S. Sunyaev, Human non-synonymous SNPs: server and survey, Nucleic Acids Res. 30 (2002) 3894–3900, https://doi.org/10.1093/nar/gkf493.
[42] P. Rentzsch, D. Witten, G.M. Cooper, J. Shendure, M. Kircher, CADD: predicting the deleteriousness of variants throughout the human genome, Nucleic Acids Res. 47 (2019) D886–D894, https://doi.org/10.1093/nar/gky1016.
[43] N. Riggi, L. Cironi, P. Provero, M.-L. Suvà, J.-C. Stehle, K. Baumer, L. Guillou, I. Stamenkovic, Expression of the FUS-CHOP fusion protein in primary mesenchymal progenitor cells gives rise to a model of myxoid liposarcoma, Cancer Res. 66 (2006) 7016–7023, https://doi.org/10.1158/0008-5472.CAN-05-3979.
[44] J.T. Robinson, H. Thorvaldsdóttir, W. Winckler, M. Guttman, E.S. Lander, G. Getz, J.P. Mesirov, Integrative genomics viewer, Nat. Biotechnol. 29 (2011) 24–26, https://doi.org/10.1038/nbt.1754.
[45] M. Sato, A.W. Liebau, Z. Liu, L. Liu, R. Rabadan, J. Gautier, The UVSSA complex alleviates MYC-driven transcription stress, J. Cell Biol. 220 (2021), https://doi.org/10.1083/jcb.201807163.
[46] C. Soneson, M.I. Love, M.D. Robinson, Differential analyses for RNA-seq: transcript-level estimates improve gene-level inferences, F1000Res 4 (2015) 1521, https://doi.org/10.12688/f1000research.7563.1.
[47] M.J. Steinbaugh, L. Pantano, R.D. Kirchner, V. Barrera, B.A. Chapman, M.E. Piper, M. Mistry, R.S. Khetani, K.D. Rutherford, O. Hofmann, J.N. Hutchinson, S. Ho Sui, bcbioRNASeq: R package for bcbio RNA-seq analysis, F1000Res 6 (2018) 1976, https://doi.org/10.12688/f1000research.12093.2.
[48] A. Subramanian, P. Tamayo, V.K. Mootha, S. Mukherjee, B.L. Ebert, M.A. Gillette, A. Paulovich, S.L. Pomeroy, T.R. Golub, E.S. Lander, J.P. Mesirov, Gene set enrichment analysis: a knowledge-based approach for interpreting genome-wide expression profiles, Proc. Natl. Acad. Sci. U. S. A. 102 (2005) 15545–15550, https://doi.org/10.1073/pnas.0506580102.
[49] E. Talevich, A.H. Shain, T. Botton, B.C. Bastian, CNVkit: genome-wide copy number detection and visualization from targeted DNA sequencing, PLoS Comput. Biol. 12 (2016), e1004873, https://doi.org/10.1371/journal.pcbi.1004873.
[50] trackViewer, A Bioconductor package for interactive and integrative visualization of multi-omics data, in: Nature Methods [WWW Document], 2021 n.d. URL https://www.nature.com/articles/s41592-019-0430-y (accessed 10.21.20).
[51] Y. van der Weegen, H. Golan-Berman, T.E.T. Mevissen, K. Apelt, R. González-Prieto, J. Goedhart, E.E. Heilbrun, A.C.O. Vertegaal, D. van den Heuvel, J. C. Walter, S. Adar, M.S. Luijsterburg, The cooperative action of CSB, CSA, and UVSSA target TFIIH to DNA damage-stalled RNA polymerase II, Nat. Commun. 11 (2020) 2104, https://doi.org/10.1038/s41467-020-15903-8.
[52] L. Wang, H.J. Park, S. Dasari, S. Wang, J.-P. Kocher, W. Li, CPAT: coding-potential assessment tool using an alignment-free logistic regression model, Nucleic Acids Res. 41 (2013) e74, https://doi.org/10.1093/nar/gkt006.
[53] X. Wang, H. Zhang, X. Chen, Drug resistance and combating drug resistance in cancer, Cancer Drug Resist. 2 (2019) 141–160, https://doi.org/10.20517/cdr.2019.10.
[54] P. Workman, E.O. Aboagye, F. Balkwill, A. Balmain, G. Bruder, D.J. Chaplin, J. A. Double, J. Everitt, D.A.H. Farningham, M.J. Glennie, L.R. Kelland, V. Robinson, I.J. Stratford, G.M. Tozer, S. Watson, S.R. Wedge, S.A. Eccles, Committee of the National Cancer Research Institute, Guidelines for the welfare and use of animals in cancer research, Br. J. Cancer 102 (2010) 1555–1577, https://doi.org/10.1038/sj.bjc.6605642.
[55] G. Yu, L.-G. Wang, Y. Han, Q.-Y. He, clusterProfiler: an R package for comparing biological themes among gene clusters, OMICS 16 (2012) 284–287, https://doi.org/10.1089/omi.2011.0118.
[56] J.S.E. Yu, Shane Colborne, Christopher S. Hughes, Gregg B. Morin, Torsten O. Nielsen, The FUS-DDIT3 Interactome in Myxoid Liposarcoma, Neoplasia 21 (2019) 740–751, https://doi.org/10.1016/j.neo.2019.05.004.